Encapsulation of Saline Solution by Tetrahydrofuran Clathrate Hydrates and Inclusion Migration by Recrystallization

Kazushige Nagashima,*,† Suguru Orihashi,† Yoshitaka Yamamoto,‡ and Masayoshi Takahashi‡

Department of Physics, School of Science and Technology, Meiji University, 1-1-1 Higashimita, Tama-ku, Kawasaki 214-8571, Japan, and National Institute of Advanced Industrial Science and Technology (AIST), 16-1 Onogawa, Tsukuba, Ibaraki 305-8569, Japan

Received: October 25, 2004; In Final Form: January 31, 2005

Encapsulation of saline solution as an impurity in tetrahydrofuran clathrate hydrates grown in a stoichiometric solution with 3 wt % NaCl and the release of a saline solution during melting along with inclusion migration by hydrate recrystallization during annealing are studied using a directional growth apparatus in combination with a Mach−Zender interferometer. Interferometric observation revealed that the salt concentration increased locally in the solution near the growth interface. The time evolution of salt concentration in the solution was in accordance with the numerical results obtained from the diffusion equation for salt, assuming perfect rejection of salt by the hydrate. However, after the interfacial pattern developed into a serrated pattern (periodical array of trough and crest), the salt concentration in the solution ceased to increase, deviating from the theoretical value. This indicates that the saline solution was encapsulated by the growth hydrate. On the other hand, upon melting of the slowly grown hydrate, the salt concentration near the interface was observed to be locally high at the location of the trough during growth, whereas it was dilute at the location of the growth crest. Furthermore, when the hydrate was annealed under an applied temperature gradient, the inclusions (encapsulated saline solution) in the hydrate migrated toward the bulk solution and were finally expelled by hydrate recrystallization. The migration speed of the inclusions increased with a larger temperature gradient. By melting the sample over a sufficiently long anneal time, the melt was determined to be completely desalinated.

1. Introduction

Clathrate hydrates are ice-like crystals composed of a hydrogen-bonded network of water molecules that contain guest molecules within cavities. Investigations of gas hydrates[1−12] have been carried out extensively due to their potential applications in solving certain energy and environmental problems. Methane hydrate, which is found globally in oceanic sediments, may prove to be a clean and viable energy resource.[4−6] The confinement of combustion gases such as carbon dioxide into deep-sea hydrates has been examined as a remedy against global warming.[7−9]

In an effort to clarify the growth and decomposition mechanism of gas hydrates, it is necessary to consider the following processes: (1) mass diffusion (guest molecules and impurities in water), (2) latent heat diffusion, (3) heat and mass transport by convection in water, (4) crystallization in porous media (i.e. oceanic sediments), (5) anisotropy of interfacial attachment kinetics (crystallographic plane dependence of incorporation kinetics of molecules into the crystal lattice sites), and others. The relations among these rate determining processes are complex, which complicates the analysis of gas hydrate experiments. To clarify the mechanisms of hydrate growth and decomposition, our strategy is to examine each process in a simplified environment which is governed by only one rate determining process. After each process has been well understood, the interrelated effects of the different rate determining processes will be examined in a complex situation relevant to the natural gas hydrates.

The effect of salt in seawater is a critical factor in understanding the hydrate growth and decomposition. To clarify the effect of salt on the stability of hydrates, phase diagrams of hydrates have been obtained in saline solutions.[10−12] However, the understanding of the diffusion process of salt adjacent to the growing and decomposing hydrates under nonequilibrium conditions is limited, because of the difficulty in quantitative measurement of the local solute concentration distribution.

Several researchers have carried out THF hydrate growth experiments.[13−17] THF is of particular utility as it is miscible with water at any molar ratio. Further, a THF−water solution system is advantageous in that a single crystal can be grown at a stoichiometrically defined THF concentration. A THF−water solution forms a structure-II hydrate[18] at atmospheric pressure below 4.4 °C.[19,20] The growth pattern of a THF hydrate single crystal is octahedral, bound by the slowest growth faces {111}. The directions of the vertices of the octahedron are in the ⟨100⟩ directions.[13−15]

In our previous study,[21,22] we focused on an idealized situation where the effect of salt diffusion was dominant by selecting an ideal solution system and suitable experimental conditions. We first succeeded in observing the salt concentration distribution adjacent to growing and melting THF hydrates in a stoichiometric THF−water solution with 3 wt % NaCl, using a directional growth apparatus combined with an interferometer. Analysis of the interferograms provided the two-dimensional distribution of the refractive index of the liquid phase. This enabled us to measure the concentration distribution of salt in the solution in-situ.[23] The salt concentration locally increased

* Corresponding author e-mail: knaga@isc.meiji.ac.jp.
† Meiji University.
‡ National Institute of Advanced Industrial Science and Technology (AIST).

10.1021/jp040680i CCC: $30.25
Published on Web 04/30/2005

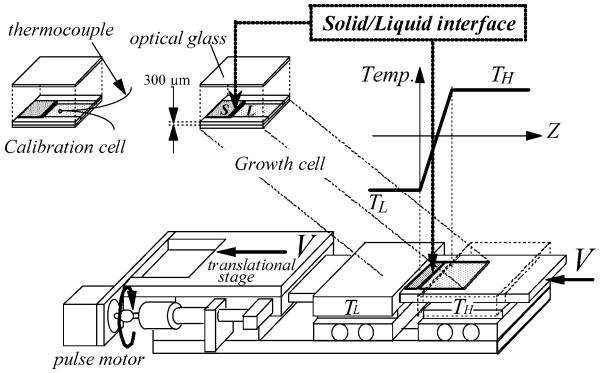

Figure 1. Schematic illustration of directional growth apparatus, growth cell, and calibration cell. The calibration cell equipped with a thermocouple is used to measure the applied temperature gradient.

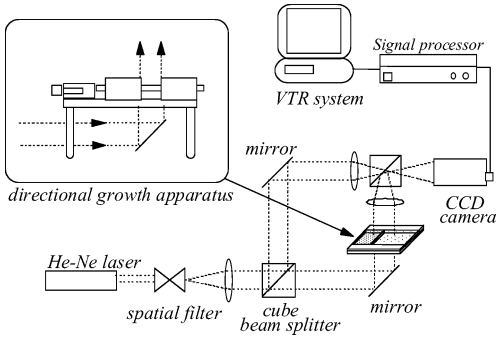

Figure 2. Schematic illustration of an optical system of a Mach−Zender interferometer in combination with a directional growth apparatus.

near the growth interface due to rejection of impurities by the hydrate. The growth process was inhibited considerably by depression of the equilibrium temperature of the hydrate. In addition, a dilute saline solution, released from the melting hydrate, caused deceleration of the melting process by raising the equilibrium temperature.

Herein, detailed interferometric observations of the salt redistribution process (rejection and encapsulation of saline solution) which occurs during the growth of THF hydrates is presented along with observations on the release of saline solution with melting, and on inclusion migration by hydrate recrystallization during annealing. Numerical calculations based on the diffusion equation for the salt in the solution assuming perfect rejection of salt by the growing hydrate were carried out in order to discuss the salt redistribution process at the growth interface.

2. Experimental Section

2.1. Sample Solution. The sample solution used was a stoichiometric THF−water solution (THF−17H_2O) supplemented with 3 wt % NaCl. Dehydrated stabilizer-free THF reagent (99.5 wt % purity, Kanto Chemical Co. Inc., Japan) and NaCl (99.5 wt % purity, Kanto Chemical Co. Inc., Japan) were used. All solutions were prepared by mixing reagents with degassed ultrapure water, prepared by deionization, distillation, and filtration.

2.2. Directional Growth Experiments. Growth, melting, and annealing experiments of THF hydrates were carried out using a directional growth apparatus (Figure 1).[21,22] The growth cell was composed of two optical glasses and spacers. The sample space in the growth cell was 14 mm × 0.3 mm × 18 mm ($w \times h \times l$). The thin sample space was chosen to reduce the mass transport by convection in the solution and enabled ideal growth conditions that were governed by the two-dimensional diffusion of salt. The growth cell was placed on two copper blocks kept −1 °C below the melting point, T_M. Hydrate crystals were nucleated in the supercooled THF−water solution. After repeated heating and cooling processes at close to T_M, one crystal survived. The vertex directions of the octahedral THF hydrate, the ⟨100⟩ directions, grew the fastest. To minimize the effect of slower growth faces (i.e. the effect of anisotropic interfacial attachment kinetics), only a successfully prepared hydrate with the fastest growth direction parallel to the forced growth direction (*Z*-axis direction in the directional growth apparatus) was used. The temperatures of the two copper blocks were changed to $T_L = -3.0$ °C (lower than T_M) and $T_H = 6.0$ °C (higher than T_M), respectively, using thermoelectric modules. The hydrate grew in the colder region, and a straight interface finally resulted at an equilibrium isotherm perpendicular to the temperature gradient applied. This procedure was carried out in the THF−water solution without salt in order to prevent encapsulation of the saline solution by the hydrate at uncontrolled growth rates. Then, the solution remaining in the sample cell was replaced by the THF−water solution with 3 wt % salt, maintaining the solution and the hydrate interface at an equilibrium temperature in order to prevent growth or melting. The hydrate was forced to grow (or melt) by moving the growth cell toward the cold block (or the hot block) at a constant velocity, *V*. The interfacial area is forced to remain at almost the same position between the two blocks due to the applied temperature gradient. The shift in the interfacial position is solely attributed to increased salt concentration and depression of the equilibrium temperature at the interface. Therefore, the growth rate of the hydrate is controlled by the velocity of the growth cell, *V*, in the steady-state condition of salt concentration distribution.

A temperature profile of the growth cell between the blocks was measured using a thermocouple in a calibration cell filled with the hydrate and solution. While the calibration cell was moved from the hot block toward the cold block at $V = 10$ μm s^{-1}, the temperature was recorded as a function of the position of the thermocouple tip. The profile was linear, regardless of latent heat emission at the growth interface. The slope of the profile, i.e., the temperature gradient *G*, was 1.8 K mm^{-1}. This indicates that the applied temperature gradient acted to rapidly remove the latent heat from the interfacial area. This apparatus is thus beneficial in preventing the effect of latent heat emission.

2.3. Optical System and Signal Processing Procedure. Figure 2 shows the optical system for the Mach−Zender interferometer used to monitor the solute concentration distribution in the solution. The reference path and the test path interfere with each other at the second cube beam splitter and produce an equidistant fringe. When the test beam is transmitted through the growth cell, where the solute concentration in the solution is two-dimensionally distributed, the two-dimensional phase distribution profile, ϕ, of the transmitted test beam produces a curved interference fringe. The phase distribution profile ϕ was obtained by analyzing the interference fringe using a signal processing procedure for the Moire phase shift interferometry.[22,24]

The refractive index difference Δn between two arbitrary points in the phase distribution profile was calculated as follows

$$\Delta n = \frac{\Lambda}{h}\frac{\Delta\phi}{2\pi} \tag{1}$$

where Λ is the wavelength of the He−Ne laser used (= 632.82 nm), *h* is the sample thickness along the laser path (= 300 μm),

and $\Delta\phi$ is the phase difference between two points. The concentration difference, ΔC, was calculated as follows

$$\Delta C = \frac{\Delta n}{\alpha} = \frac{\Lambda}{h\alpha}\cdot\frac{\Delta\phi}{2\pi} \tag{2}$$

where α is the coefficient in the calibration line of a refractive index as a function of the solute concentration: $n(C) = n(0) + \alpha\cdot C$, which was obtained in our previous study for the stoichiometric THF−water solution as a function of the salt concentration C at 4.4 °C as $n(C) = 1.3544 + 1.62 \times 10^{-3}\cdot C$.[22]

Considering the refractive index difference between an arbitrary point and a point far from the interface, the two-dimensional concentration distribution of salt, C, was obtained as follows

$$C = C_0 + \frac{\Delta n}{\alpha} = C_0 + \frac{\Lambda}{h\alpha}\cdot\frac{\Delta\phi}{2\pi} \tag{3}$$

where the salt concentration at a position far away from the hydrate (i.e. a standard value) must always be at the initial concentration of C_0 (= 3 wt %). During all experiments as well as measuring the interfacial region we observed that the phase distribution profile in the far-away region (at extreme right of image) was uniform (no salt concentration gradient) to ensure that the salt concentration at the standard position did not vary from C_0. However, after the stop of the growth experiment in the solution with salt before the melting and annealing experiments, the dense saline solution rejected by the growth interface diffused toward the bulk solution and increased the standard value (the salt concentration gradient was observed at the standard position). Unfortunately, the present system cannot monitor the temporal shift in the standard value. This was because a baseline (i.e. a uniform phase distribution profile in a blank cell) oscillated in a parallel fashion, despite minimization of interferometer vibration by using an optical table with vibration isolators. To compensate for this, the solution remaining in the sample cell was replaced by the initial sample solution at C_0 before the melting and annealing experiments on the grown hydrates.

2.4. Experimental Procedure. The time evolution of the growth pattern and the salt concentration distribution in the solution near the growth hydrate were first observed in order to clarify the saline solution rejection and encapsulation processes of the hydrate. The amount of saline solution inclusions encapsulated by the hydrate cannot be directly evaluated by interferometry; therefore, samples grown at various conditions were melted into the liquid phase. The salt concentration distribution in the melt along the interface was observed by the interferometer. The effects of the hydrate growth rate, V, and the anneal time (premelting hold time) at $V = 0$ were evaluated. The melting rate was fixed at $V_M = -5\ \mu\text{m s}^{-1}$ (the negative sign indicates the movement of the sample cell in the direction opposite to the growth process). In addition, the inclusion migration by hydrate recrystallization during annealing was directly observed using an optical microscope. The expelling of inclusions into the bulk solution during annealing was observed by the interferometer.

3. Results

3.1. Growth Process of Hydrate. Figure 3 shows the time sequence phase distribution profiles displaying the interfacial pattern and the concentration distribution of salt in front of the growing hydrate at $V = 1\ \mu\text{m s}^{-1}$.[22] The growth times are (a) $t = 0$ s, (b) $t = 900$ s, (c) $t = 1500$ s, (d) $t = 3000$ s, and (e) $t = 4500$ s. The interfacial pattern at $V = 0$ was straight along an isotherm perpendicular to the applied temperature gradient (Z-axis direction) (Figure 3a). The concentration distribution in the solution was uniform at the initial concentration, $C_0 = 3$ wt %. When the growth cell was moved toward the cold block (-Z-axis direction) at the constant V, the hydrate initiated growth. Figure 3b−d shows the evolution of undulations at the straight interface. The interfacial position gradually moved to the colder region in the -Z-axis direction as visualized under the microscope. This was a result of the depression of the equilibrium temperature due to the increase in the salt concentration at the interface in the solution. Figure 3e shows the formation of an orderly serrated pattern (periodical array of trough and crest) bound by the slowest growth faces of {111}. Finally, the interfacial position was observed to be at a fixed position under the microscope. The growth rate of the crystal corresponded with the velocity of the sample cell, V.

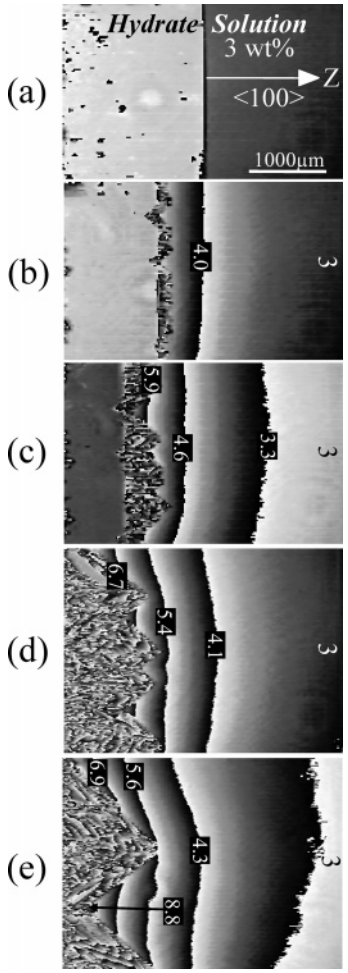

Figure 3. Sequence of images of the interfacial pattern and the salt concentration distributions near THF hydrate growing at $V = 1\ \mu\text{m s}^{-1}$. The growth times are (a) $t = 0$ s, (b) $t = 900$ s, (c) $t = 1500$ s, (d) $t = 3000$ s, and (e) $t = 4500$ s. The numbers in the images show the salt concentration in the solution.

The gray scale level of phase distribution in solution reflects the distribution of the salt concentration. According to eq 3, a phase difference of 2π (the gray scale level changes from black to white in the image) corresponds to a concentration change of 1.3 wt %. The numbers in the images show the salt concentration in the solution. Note that the gray scale levels at the extreme right of the images are not constant. This is due to the baseline oscillation of the phase distribution profile. The

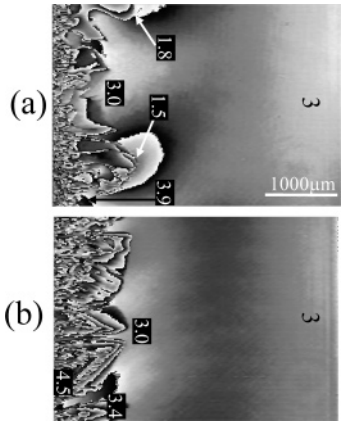

Figure 4. Images for the melting pattern and the salt concentration distribution in the solution close to the melting hydrate at $V_M = -5$ μm s^{-1} at a melting time of $t = 600$ s. The hydrate samples were prepared at (a) $V = 1$ μm s^{-1} and (b) $V = 10$ μm s^{-1}. The anneal time at $V = 0$ before melting was 0 h.

salt concentration at the extreme right was confirmed to be C_0 by the procedure described in Section 2.3.

The results indicate that when the hydrate began to grow, the salt concentration gradually increased near the interface due to the rejection of salt by the hydrate. The salt concentration was the highest at the growth interface and decreased exponentially down to the initial concentration C_0 ahead of the interface. The salt concentration reached 5.6 wt % at the crest of the growth interface and more than 8 wt % in the trough (Figure 3e).

3.2. Melting Process of Hydrate. Figure 4 shows a sequence of the interfacial melting pattern and the salt concentration distribution near the melting hydrate at $V_M = -5$ μm s^{-1} at a melting time of $t = 600$ s. The hydrate samples were prepared at a growth rate of (a) $V = 1$ μm s^{-1} and (b) $V = 10$ μm s^{-1}. The anneal time (i.e. premelting hold time) at $V = 0$ is 0 h.

The melting interfacial pattern was undulated. Specific crystallographic planes were not observed. However, the positions of the fastest melting position and the slowest melting position corresponded to the previous trough and crest exhibited during growth. The melting interface of the slowly grown hydrate (Figure 4a) was more undulated than that of the faster grown hydrate (Figure 4b). The salt concentration released from the melting hydrate at the previous trough was about 4 wt % or higher. The salt concentration at the previous crest was determined to be more dilute during melting of the slower grown hydrate, $C = 1.5$ wt % (Figure 4a). Therefore, the salt concentration variation along the melting interface was larger in the case of melting of the slower grown hydrate. When the salt concentrations during melting ($C = 1.5$ wt % at the crest and $C = 3.9$ wt % in the trough (Figure 4a)) were compared with the concentrations during growth ($C = 5.6$ wt % at the crest and $C = 8.8$ wt % in the trough (Figure 3e)), it was found that 27% of salt at the crest and 44% of salt in the trough were encapsulated by the growing hydrate. Results indicated that the growth hydrate encapsulated denser and more saline solution in the trough than the hydrate at the crest.

3.3. Annealing of Hydrates at $V = 0$. Figure 5 shows the sequent images of expelling of the trapped saline solution from the hydrate into the bulk liquid region during annealing at $V = 0$ under an applied temperature gradient. The hydrate sample was prepared at $V = 10$ μm s^{-1}. The anneal times are (a) 5 min, (b) 60 min, (c) 180 min, and (d) 300 min. The white curve in the solution region indicates the gray level change along the dashed line.

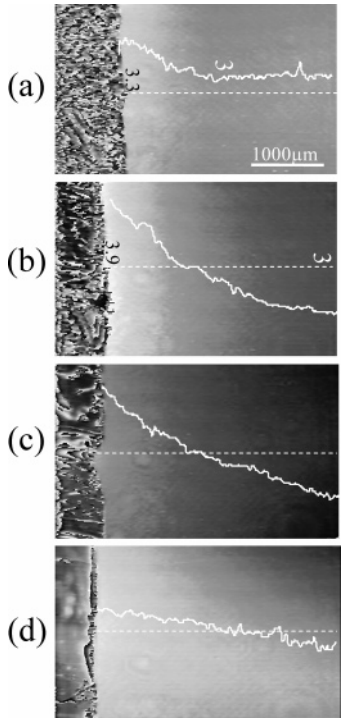

Figure 5. Sequence images of expelling of the trapped saline solution from the hydrate into the bulk liquid region during annealing of the hydrate at $V = 0$ under an applied temperature gradient. The hydrate sample was prepared at $V = 10$ μm s^{-1}. The anneal times are (a) 5 min, (b) 60 min, (c) 180 min, and (d) 300 min.

In Figure 5a, the salt concentration near the interface began to increase. This increase indicates that the saline solution was expelled from the hydrate during annealing at $V = 0$. The salt concentration in the solution gradually increased near the interface, and a diffusion field of salt developed in the solution (Figure 5b). In parts c and d of Figure 5, the saline solution diffused over to the extreme right of the images. The salt concentration at the interface cannot currently be analyzed unless the standard value of C_0 is maintained in the region far from the interface. The concentration gradient of salt at the interface, indicated by the white curve in Figure 5c, revealed that the expelling process continued. The decrease in the concentration gradient in Figure 5d, however, indicated that the expelling process decelerated with time.

The gray scale image in the hydrate shows qualitatively the amount of the saline solution in the hydrate. In Figure 5a, the gray scale distribution is disordered. The gray scale distribution gradually smoothed out in Figure 5b,c, corresponding to recrystallization in the hydrate by expelling the saline solution. The gray scale distribution in the hydrate in Figure 5d became almost uniform, indicating the formation of a uniform single crystal with few saline solution inclusions.

Figure 6 shows the sequent images of the hydrate observed by an optical microscope during annealing at $V = 0$. The hydrate was prepared at $V = 10$ μm s^{-1}. The anneal times are (a) 1 h, (b) 3 h, (c) 5 h, (d) 11 h, (e) 13 h, (f) 15 h, and (g) 24 h. The crystal surface parallel to the glass cell was stepped, as shown in Figure 6a. As time elapsed, the sharp stepped pattern was coarsened by further crystallization in gaps in the hydrate, expelling the saline solution into the bulk liquid region (Figure 6b). The saline solution in the hydrate region was finally encapsulated as inclusions without channels of solution connected to the bulk liquid region (Figure 6c). The inclusions slowly migrated toward the bulk liquid region, as shown in Figure 6c−f. Circles in the figures indicate the inclusion

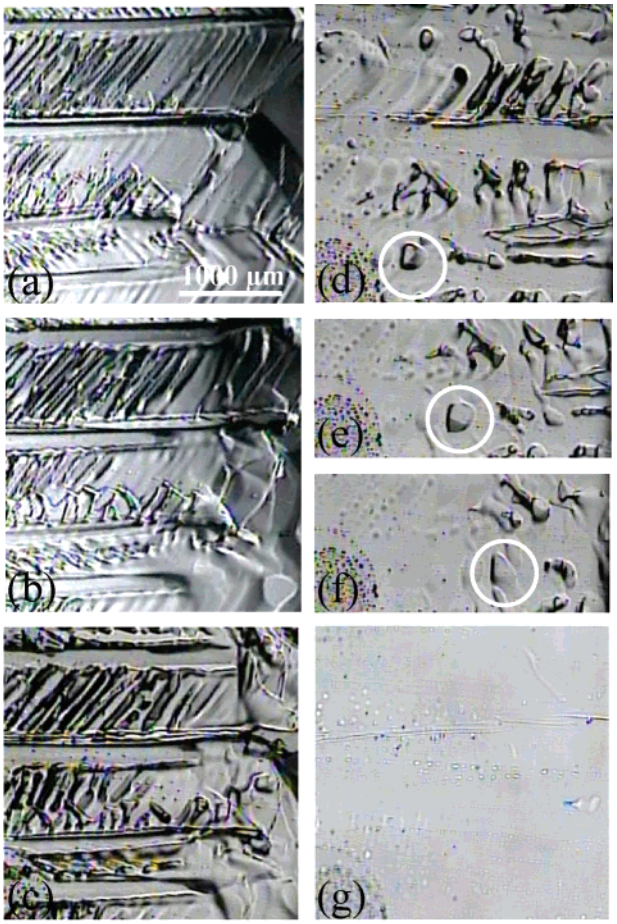

Figure 6. Sequence of images of the hydrate observed by an optical microscope during annealing at $V = 0$. The hydrate was prepared at $V = 10\ \mu\text{m s}^{-1}$. The anneal times are (a) 1 h, (b) 3 h, (c) 5 h, (d) 11 h, (e) 13 h, (f) 15 h, and (g) 24 h.

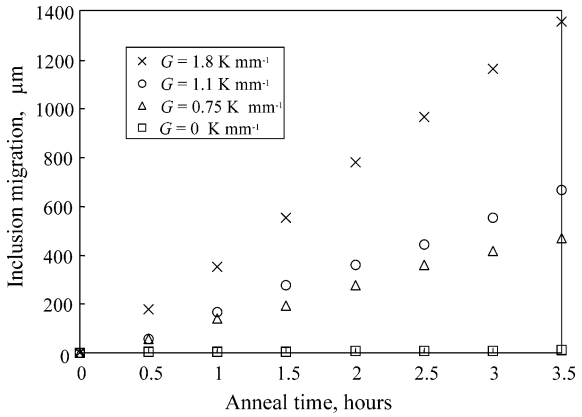

Figure 7. Inclusion migration as a function of anneal time at various values of temperature gradient, G.

migrating toward the hotter region. All the inclusions migrated together at a uniform speed. Finally, after 24 h annealing (Figure 6g), all the inclusions were expelled into the liquid region, and a uniform hydrate was formed.

Figure 7 shows the effect of the applied temperature gradient G on the inclusion migration as a function of the anneal time at $V = 0$. At a fixed value of G, the inclusions moved at a constant speed toward the hotter region in the hydrate. The migration speed decreased at the smaller value of G. When G was changed to 0 at $T_H = T_L = -3.1$ °C (below T_M), the migration of inclusions stopped. This result explicitly indicated

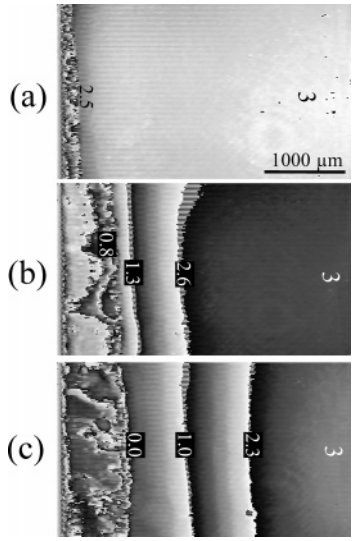

Figure 8. Sequence of images of interfacial patterns and the salt concentration distribution near the melting hydrate at $V_M = -5\ \mu\text{m s}^{-1}$. The hydrate sample was prepared at $V = 10\ \mu\text{m s}^{-1}$. The anneal time at $V = 0$ before melting was 24 h. The melting times are (a) $t = 200$ s, (b) $t = 400$ s, and (c) $t = 600$ s.

that the migration of inclusions was caused by the effect of the applied temperature gradient.

3.4. Melting Process after 24 h Annealing. Figure 8 shows sequent images of the interfacial pattern and the salt concentration distribution near the melting hydrate at $V_M = -5\ \mu\text{m s}^{-1}$.[22] The hydrate sample was prepared at $V = 10\ \mu\text{m s}^{-1}$ and was annealed at $V = 0$ at $G = 1.8\ \text{K mm}^{-1}$ for 24 h. The melting times are (a) $t = 200$ s, (b) $t = 400$ s, and (c) $t = 600$ s. In contrast to the results without annealing as shown in Figure 4, the interfacial pattern was almost straight along the isotherm perpendicular to the temperature gradient direction. The salt concentration in the melt near the hydrate decreased gradually. The contours of the salt concentration distribution were almost parallel to the straight interface. Finally, the salt concentration at the interface decreased to 0 wt %. Hydrate annealed over a sufficiently long time under the applied temperature gradient was determined to be completely desalinated.

4. Discussion

4.1. Theoretical Background. To discuss the rejection and the encapsulation of salt in the solution by the growing hydrate, the time evolution of the salt concentration at the growth interface in the solution will be compared with theoretical results which only take into account the effect of salt diffusion in the solution. The expression of salt diffusion in the solution and the boundary conditions governing the evolution of our system are given as follows

$$D\frac{\partial^2 C}{\partial^2 Z} + V\frac{\partial C}{\partial Z} = \frac{\partial C}{\partial t} \tag{4}$$

where $C(Z, t)$ is the time dependent concentration field ahead of the interface, Z is the displacement along the Z-axis in a frame moving at V with respect to the growing hydrate, and D is the diffusion coefficient of salt in the solution. There are several boundary conditions that must be satisfied. Assuming a local equilibrium condition at the interface, we require

$$C(Z_{\text{int}},t) = -\frac{G}{m}Z_{\text{int}} \tag{5}$$

where Z_{int} is the position of the interface and m is the magnitude of liquidus slope in the phase diagram. When the salt concentration increases at the growth interface, the interfacial position moves toward the colder region, due to depression in the equilibrium temperature. Therefore, the interfacial position Z_{int} is always in the region $Z < 0$. In the non-steady state prior to the establishment of a steady-state concentration distribution of salt, the actual growth rate of the crystal, R, in the frame of reference that is fixed in the growing hydrate is

$$R(t) = V + \dot{Z}_{int}(t) \tag{6}$$

Finally, the conservation law of solutes at the interface requires

$$-D\left.\frac{\partial C}{\partial Z}\right|_{Z_{int}} = R(1-k)C(Z_{int},t) \tag{7}$$

where k is the segregation coefficient, which is the ratio of the salt concentration incorporated in the crystal lattice sites to the salt concentration at the growth interface in the solution.

We must solve the system of eqs 4−7 for fixed $V > 0$ and initial conditions appropriate to the stationary interface at $V = 0$

$$C(Z,0) = \begin{cases} C_0, Z > Z_{int}(0) \\ kC_0, Z < Z_{int}(0) \end{cases} \tag{8}$$

Since no analytical solution to this version of the Stefan problem is known, a boundary layer approximation was proposed by Warren et al.,[25] as follows. In the steady state, the concentration profile ahead of a straight interface moving at a constant movement velocity is

$$C_V(Z) = C_0 + \left[\frac{C_0}{k} - C_0\right]e^{-2(Z-Z_0/k)/l_V} \tag{9}$$

where the diffusion length of solute l_V is

$$l_V = \frac{2D}{V} \tag{10}$$

Z_0 is the steady-state position of the straight interface in the moving frame

$$Z_0 = -\frac{m}{G}C_0 \tag{11}$$

Considering eq 9, it seems plausible to assume that the non-steady-state concentration profile can be approximated by a function of the form

$$C(Z,t) = C_0 + [C(Z_{int},t) - C_0]e^{-2(Z-Z_{int})/l} \tag{12}$$

where l is now a time dependent parameter describing the thickness of the concentration boundary layer, and $Z_{int}(t)$ is the instantaneous position of the interface.

The coupled partial differential equations eqs 13 and 14 are derived as follows

$$R(t) = V + \dot{Z}_{int} = \frac{2D(Z_{int} - Z_0)}{l(1-k)Z_{int}} \tag{13}$$

$$\dot{l} = \frac{4D(Z_0 - kZ_{int})}{l(1-k)Z_{int}} - \frac{l}{Z_{int} - Z_0}\dot{Z}_{int} \tag{14}$$

Eqs 13 and 14 are numerically calculated using the values $D = 1.23 \times 10^{-5}$ cm^2 s^{-1},[22] $m = 0.89$ K wt %$^{-1}$,[26] and $k = 0$ (perfect rejection of salt by the hydrate as impurity). The salt concentration at the growth interface $C_{int}(t)$ ($= C(Z_{int}, t)$) is obtained from the result of Z_{int} using eq 5, as shown by the solid curves in Figure 9.

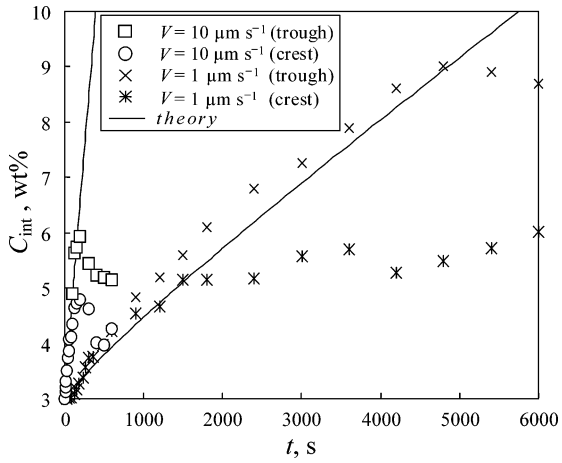

Figure 9. The time evolution of salt concentration at the growth interface at $V = 1$ μm s^{-1} and 10 μm s^{-1}. After the serrated interfacial pattern started to form ($t > 600$ s at $V = 1$ μm s^{-1} and $t > 60$ s at $V = 10$ μm s^{-1}), the salt concentration at the crest and the trough were plotted. The theoretical results are shown by the solid curves.

4.2. Time Evolution of Salt Concentration at the Growth Interface. The time evolution of the salt concentration at the growth interface was experimentally obtained from the time sequence images of the concentration profiles (Figure 3). The experimental results for $V = 1$ μm s^{-1} and $V = 10$ μm s^{-1} are plotted in Figure 9. After the serrated interfacial pattern started to form ($t > 600$ s at $V = 1$ μm s^{-1} and $t > 60$ s at $V = 10$ μm s^{-1}), the salt concentration at the crest and the trough were plotted. The theoretical results are shown by the solid curves.

The salt concentration at the interface C_{int} rapidly increased as the hydrate started to grow. The increasing rate of C_{int} was larger at higher growth rates. At the initial stage of growth, when the growth interface was almost straight (shown in Figure 3a,b), the experimental results were in good agreement with those of the theoretical results, assuming a one-dimensional diffusion of salt in the solution and the perfect rejection of salt by the hydrate.

After the serrated interfacial pattern started to form, experimental results indicated that an increase in C_{int} suddenly dropped at the growth crest ($t > 1500$ s at $V = 1$ μm s^{-1}). Further, at the growth crest, C_{int} became plateaued. On the other hand, C_{int} at the trough continued to increase ($1500 < t < 4800$ s). C_{int} at the crest was lower than the theoretical results, whereas that at the trough was higher than the theoretical results. This is thought to be due to the radial diffusion of salt from the crest not only toward the growth direction but also toward the trough. Figure 3 shows that the lines of contour for the salt concentration are not straight but are curved near the crest due to the radial diffusion of salt. This is thought to be a limitation of theoretical predictions assuming a one-dimensional diffusion in the Z-axis direction.

At the final stage of growth, the salt concentration at the trough was saturated ($t > 4800$ s at $V = 1$ μm s^{-1}), whereas the theoretical value continued to increase. When the segregation coefficient k is 0, the theoretical model results in a further increase in the salt concentration at the growth interface. The saturation of the experimental results for C_{int} concludes that the dense saline solution at the interface was encapsulated by the hydrate.

4.3. Migration of Saline Inclusions. The migration of saline inclusions in the hydrate, as shown in Figures 6 and 7, was determined to be caused by the effect of the applied temperature gradient. When the salt concentration in the inclusions was uniformly mixed due to solute diffusion, the interface with the hotter region in the inclusions melts. The salt concentration in the inclusions in the hotter region decreases by releasing salt-free THF−water solution from the hydrate. The inclusions are small enough for the dilute saline solution in the hotter region to mix with the solution in the colder region. Thus, raising of the equilibrium temperature by dilution of the solution causes growth of the interface with the colder region. The growth in the colder region causes an increase in salt concentration in the inclusions. This decreases the growth rate in the colder region. However, when the melting in the hotter region is faster than the growth in the colder region, the salt concentration in the inclusions gradually dilutes, expanding the volume of the inclusions. Thus the equilibrium temperature for the salt concentration gradually increases. This results in the migration of inclusions in the hydrate under the applied temperature gradient at $G > 0$ and ultimate expelling of saline solution inclusions into the bulk liquid region.

In the present experimental conditions, expansion of the inclusion volume was not clearly observed even at the highest value of G applied with the present apparatus. In addition, the inclusion shapes were irregular, which makes the analysis imprecise. Spherical inclusions should be prepared for precise measurement of the volume change and be observed under a higher applied temperature gradient to enhance the expansion speed of inclusions. In addition, not only the effect of the temperature gradient but also the effect of the actual temperature must also be an important factor. When the inclusion migration is observed over a longer time scale or at a larger value of G, the inclusion migration speed may change depending on the increase in the actual temperature and the increase in the inclusion volume. These effects will be demonstrated using an improved setup under suitably selected experimental conditions and will be reported soon in a separate paper.

5. Conclusions

Encapsulation of saline solution by growing tetrahydrofuran clathrate hydrates in stoichiometric solution with 3 wt % NaCl, release of saline solution during melting, and inclusion migration during annealing by hydrate recrystallization were investigated using a directional growth apparatus in combination with an interferometer. A comparison between theoretical and experimental results for the time evolution of the salt concentration at the growth interface revealed that the dense saline solution was encapsulated by the growing hydrate. The undulated melting pattern and the salt concentration in the melt indicated that during the growth process the hydrate encapsulated a denser, more saline solution in the growth trough than the hydrate did at the crest. Optical microscope images explicitly indicated that the migration of saline inclusions in the hydrate was caused by the effect of the applied temperature gradient. During melting of the hydrate after a sufficiently long anneal time at $V = 0$ under an applied temperature gradient, the melt was completely desalinated. The salt concentrations near the melting hydrates not subject to annealing (Figures 4) and those over 24-h annealing (Figures 8) were determined to differ by more than 4 wt %, depending on the hydrate sample conditions before melting. The salt concentration difference at the interface caused a melting temperature difference of 3.6 °C ($= m\Delta C$), which is thought to have a significant effect on the melting rate of the hydrates. The growth velocity, the anneal time, and the magnitude of the applied G were determined to be critical factors in determining the melting rate of the hydrate.

References and Notes

(1) Sloan, E. D., Jr. *Clathrate hydrates of natural gases*, 2nd ed.; Marcel Dekker Inc.: New York, USA, 1998.

(2) Makogon, Y. F. *Hydrates of hydrocarbons*, 2nd ed.; Pennwell Publishing Company: Tulsa, Oklahoma, USA, 1997.

(3) Englezos, P. *Clathrate hydrates-review*. *Ind. Eng. Chem. Res.* **1993**, *32*, 1251.

(4) Kvenvolden, K. A. *Chem. Geol*. **1988**, *71*, 41.

(5) MacDonald, G. J. *Annu. Rev. Energy* **1990**, *15*, 53.

(6) Holder, G. D.; Kamath, V. A.; Godbole, S. P. *Annu. Rev. Energy* **1984**, *9*, 427.

(7) Uchida, T. *Waste Mgmt*. **1997**, *17*, 343.

(8) Uchida, T.; Ebinuma, T.; Kawabata, J.; Narita, H. *J. Cryst. Growth* **1999**, *204*, 348.

(9) Mori, Y. H. *Energy Convers. Mgmt*. **1998**, *39*, 1537.

(10) de Roo, J. L.; Peters, C. J.; Lichtenthaler, R. N.; Diepen, G. A. M. *AIChE J*. **1983**, *29*, 651.

(11) Kobayashi, R. Ph.D. Dissertation, U. Mich., University Microfilms No. 3521, Ann Arbor, MI, 1951.

(12) Vlahakis, J. G.; Chen, H. S.; Suwandi, M. S.; Barduhn, A. J. *Syracuse U. Research and Development Report 830, US Department of the Interior*, Nov., 1972.

(13) Makogon, T. Y.; Larsen, R.; Knight, C. A.; Sloan, E. D., Jr. *J. Cryst. Growth* **1997**, *179*, 258.

(14) Larsen, R.; Knight, C. A.; Sloan, E. D., Jr. *Fluid Phase Equilibria* **1998**, *150*, 353.

(15) Knight, C. A.; Rider, K. *Philos. Mag. A* **2002,** *82*, 1609.

(16) Devarakonda, S.; Groysman, A.; Myerson, A. S. *J. Cryst. Growth* **1999**, *204*, 525.

(17) Iida, T.; Mori, H.; Mochizuki, T.; Mori, Y. H. *Chem. Eng. Sci.* **2001**, *56*, 4147.

(18) Mak, T. C. W.; McMullan, R. K. *J. Chem. Phys.* **1965**, *42*, 2732.

(19) Hanley, H. J. M.; Meyers, G. J.; White, J. W.; Sloan, E. D. *Int. J. Thermophys*. **1989**, *10*, 903.

(20) Handa, Y. P.; Hawkins, R. E.; Murray, J. J. *J. Chem. Thermodyn.* **1984**, *16*, 623.

(21) Nagashima, K.; Yamamoto, Y.; Komai, T.; Hoshino, H.; Ohga, K. *Jpn., J. Inst. Energy* **1999**, *78*, 325.

(22) Nagashima, K.; Yamamoto, Y.; Takahashi, M.; Komai, T. *Fluid Phase Equilibria* **2003**, *214*, 11.

(23) Nagashima, K.; Furukawa, Y. *J. Phys. Chem. B* **1997**, *101*, 6174.

(24) Kanzaki, N.; Onuma, K.; Ito, A.; Teraoka, K.; Tateishi, T.; Tsutsumi, S. *J. Phys. Chem. B* **1998**, *102*, 6471.

(25) Warren, J. A.; Langer, J. S. *Phys. Rev. E* **1993**, *47*, 2702.

(26) Nagashima, K.; Yamamoto, Y.; Takahashi, M.; Komai, T. *Sci. Technol. High Pressure* **2000**, *1*, 573.